Matrix-Bound Nanochemical Possibilities

Paul A. Anderson,[†] Robert G. Bell,[‡] C. Richard A. Catlow,[‡] Fuh Lim Chang,[§] Andrew J. Dent,[⊥] Peter P. Edwards,[†] Ian Gameson,[†] Itasham Hussain,[†] Adrian Porch,[§] and John Meurig Thomas[‡]

School of Chemistry, University of Birmingham, Edgbaston, Birmingham, B15 2TT, U.K.; The Royal Institution of Great Britain, 21 Albemarle Street, London W1X 4BS, U.K.; School of Electronic and Electrical Engineering, University of Birmingham, Edgbaston, Birmingham B15 2TT, U.K.; and Daresbury Laboratory, Daresbury, Warrington, Cheshire WA4 4AD, U.K.

Received February 28, 1996. Revised Manuscript Received June 11, 1996[⊗]

In this paper we highlight through two examples the potential of zeolitic host materials for the production of totally engineered macroscopic-scale electronic structures that are made up of vast arrays of reduced dimensionality subunits. Through a novel contactless microwave cavity technique we have investigated the electrical conductivity and dielectric properties of a mesoscopic assembly of ultrafine (atomic-scale) wires of potassium prepared within a highly structured aluminosilicate matrix, zeolite L. We have observed an increase in room-temperature conductivity of around 5 orders of magnitude relative to unmodified zeolite, which may be ascribed to thermally activated electronic conduction. In our second example, a combined X-ray/EXAFS study has provided valuable insights into the reduction process involved in the preparation of nanoscale ferromagnetic cobalt particles in zeolite X. In addition, detailed calculations of cation solvation energies represent the first attempt to explain the driving force behind the two important and related chemical processes—namely the dissolution of elemental metals and ionic salts in dehydrated zeolites—used to incorporate metal species into the zeolite matrix in these two cases.

Introduction

A number of years ago, in the former Soviet Union, Bogomolov and Agroskin and co-workers[1−5] showed that it was possible to force materials such as lead, thallium, and mercury into the channels of single crystals of natural mordenite (idealized formula $M_xAl_8Si_{40}O_{96}$), the diameter of the main channels running perpendicular to the plane of the 12-rings and parallel to the *c*-axis being ca. 7.4 Å. Chains of selenium, which they also succeeded in incorporating into the channels of the host matrix, exhibited strong anisotropy in their optical spectrum. Later work by Terasaki et al.[6−9] confirmed, both by high-resolution electron microscopy[6] and by Rietveld profile refinement of X-ray powder diffractograms[8] that isolated individual chains of selenium could indeed be incorporated into the channels of mordenite and that the element was taken up as parallel double chains into the channels of zeolite L.

One of the principal stimuli for the work of Terasaki et al. stemmed from the disappointments associated with prior studies of low-dimensional solids when it was realized that relatively few of the investigated systems exhibit genuine one- (or even two-) dimensional behavior. Measured electronic and optical properties of crystalline and amorphous low-dimensional solids signified that there was significant interchain or interlayer perturbation. The scope offered by a dielectric matrix such as mordenite therefore seemed attractive. The incorporation of the selenium as individual chains was found to transform the white mordenite into an orange color.

With zeolites X, Y, and A that have cavities (rather than continuous channels as in mordenite or zeolite L), selenium tends to be occluded as pairs of Se_8 rings rather than isolated chains, and the resulting compounds have less interesting optical properties. But when binary compounds such as those of cadmium chalcogenides (CdS or CdSe) or transition-metal oxides such as Co_xO_y or spinels are accommodated as nanoparticles inside the sodalite cage of zeolites A or Y, extremely interesting optical (and photocatalytic) properties arise.[10] As early as 1989, Herron, Stucky, and co-workers[11] reported a determination (by X-ray Rietveld profile refinement—cf. ref 8) of the structure of Cd_4S_4 nanoparticles accommodated inside a sodalite cage.

[†] School of Chemistry, University of Birmingham.
[‡] The Royal Institution of Great Britain.
[§] School of Electronic and Electrical Engineering, University of Birmingham.
[⊥] Daresbury Laboratory.
[⊗] Abstract published in *Advance ACS Abstracts,* August 15, 1996.

(1) Bogomolov, V. N. *Sov. Phys. Usp.* **1978**, *21*, 77.
(2) Agroskin, L. S.; Bogomolov, V. N.; Gutman, A. I.; Zadorozhnii, A. I.; Rautian, L. P.; Romanov, S. G. *JETP Lett.* **1981**, *31*, 583.
(3) Bogomolov, V. N.; Poborchii, V. V.; Kholodkevich, S. V.; Shagin, S. I. *JETP Lett.* **1984**, *38*, 532.
(4) Bogomolov, V. N.; Poborchii, V. V.; Romanov, S. G.; Shagin, S. I. *J Phys. C Solid State Phys.* **1985**, *18*, L313.
(5) Bogomolov, V. N.; Kholodkevich, S. V.; Romanov, S. G.; Agroskin, L. S. *Solid State Commun.* **1983**, *47*, 181.
(6) Terasaki, O.; Yamazaki, K.; Thomas, J. M.; Ohsuna, T.; Watanabe, D.; Sanders, J. V.; Barry, J. C. *Nature* **1987**, *330*, 58.
(7) Terasaki, O.; Yamazaki, K.; Thomas, J. M.; Watanabe, D. *Inst. Phys. Conf. Ser., No. 93*, Vol. 2, p 297.
(8) Terasaki, O.; Shiokawn, K.; Ito, M.; Yamazaki, K.; Thomas, J. M. "*Zeolites: Facts, Figures, Future*; Jacobs, P. A., van Santen, R. A., Eds.; Elsevier: Amsterdam, 1989; p 431.
(9) Nozue, Y.; Kodaira, T.; Terasaki, O.; Yamazaki, K.; Goto, T.; Watanabe, D.; Thomas, J. M. *J. Phys. Condensed Matter* **1990**, *2*, 5209.
(10) Stucky, G. D.; MacDougall, J. E. *Science* **1990**, *247*, 669.
(11) Herron, N.; Wang, Y.; Eddy, M. M.; Stucky, G. D.; Cox, D. E.; Moller, K.; Bein, T. *J. Am. Chem. Soc.* **1989**, *111*, 530.

S0897-4756(96)00167-6 CCC: $12.00

The key significance of the ability to have well-defined nanoparticles of binary compounds (such as Cd_4S_4) inside a zeolitic matrix stems from the optical and electronic consequences. Because of the operation of a quantum size effect highlighted by the work of Brus,[12] Henglein,[13] and others,[14] the bandgap of a given binary solid may be *systematically* varied since it is inversely proportional to the nanoparticle size. Advantage may be taken of this fact, in a photocatalytic context,[14] for example, so as to render a solid, which in its bulk state does not straddle a particular set of redox potentials, to do so when prepared as a nanoparticle.

The fabrication of reduced dimensionality, nanoscale electronic structures represents one of the most formidable challenges in the science and technology of functional materials. The goal for the new millenium must be to produce totally engineered macroscopic-scale structures that are made up of vast arrays of reduced dimensionality subunits. Our aim here is to highlight the potential of zeolitic host matrixes in this quest. It is clear from the work adumbrated above that zeolite frameworks have enormous potential as molecular scaffolding for the chemical synthesis of ordered assemblies of finely divided fragments of a wide range of solid-state materials. Crucially these include arrays of quasi-one-dimensional (quantum wire) and quasi-zero-dimensional (quantum dot) structures, which cannot yet be prepared without significant size fluctuation by other means.

The task of synthesizing fragments of optically, electronically, or magnetically interesting materials within the intracrystalline pore space of zeolite matrixes is tractable only on account of the rich chemistry of the framework materials themselves. In this paper, we describe how we have exploited two important chemical processes to this end. First we show how the ionization of potassium metal inside the one-dimensional framework of zeolite L leads to a spectacular increase in room-temperature conductivity, lending credence to the suggestion that it may be possible to effect a matrix-bound insulator−metal transition resulting in a dense ordered array of one-dimensional conducting wires.[15−18] Second, we demonstrate the efficacy of salt occlusion in introducing cobalt species into zeolite X[19] and describe the subsequent reduction of the resulting compounds to produce finely divided ferromagnetic cobalt particles. Through detailed calculations of cation solvation energies, we shall for the first time attempt to develop a rigorous explanation for the driving force behind these two related processes.

Dissolving Potassium in Zeolite L

In two timely publications, Kelly[20,21] has recently highlighted the poor prospects for practical quasi-one-dimensional electronic devices emerging from existing fabrication technologies. One of the proposed radical alternatives, viewed from a long-term perspective, relates to the concept of "crystal engineering" in the fabrication of such devices. In this context, metal-loaded zeolites have recently been identified[21] as promising candidates in the search for a dense bundle ($\gg 10^6$ cm^{-2}) of quasi-one-dimensional wires (Figure 1). In dehydrated potassium zeolite L, for example, cations coordinated on only one side to an anionic framework, line the inside of a series of regular channels, into which the controlled and continuous doping of "excess electrons" is possible through their reaction with potassium vapor.[16−18] We have noted that at some critical stage of metal doping, one expects enhanced electron−electron interactions and the possibility of an insulator−metal transition.[15]

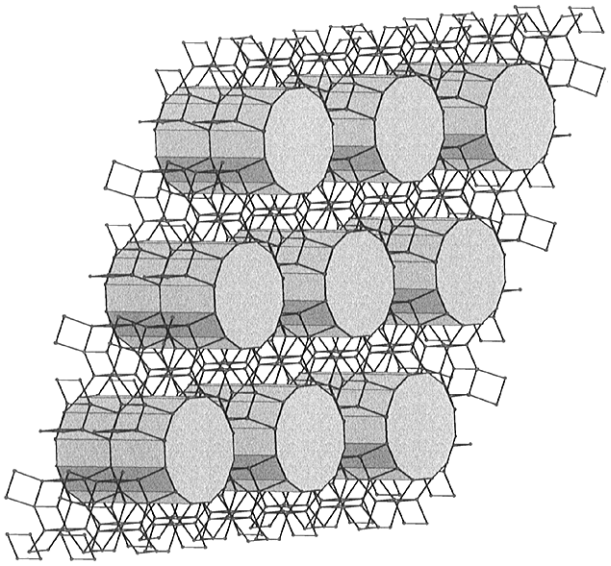

Figure 1. Representation of the structure of zeolite L highlighting the closely packed one-dimensional channel structure in which a dense bundle of nanoscale wires might be assembled.

The compounds K_x/K_9-L (x = 1, 3, 5, 7, 9) were prepared through the reaction of dehydrated potassium zeolite LTL (K_9-L), supplied by Laporte, with an amount of potassium vapor equivalent to x potassium atoms per zeolite unit cell. The reactions were carried out at temperatures between 200 and 250 °C in sealed, evacuated quartz reaction tubes, as described previously.[22,23] Careful annealing resulted in homogeneous blue solids, with the intensity of the color increasing with the amount of added metal. Full characterization of the compounds through electron spin resonance (ESR) and powder neutron diffraction studies is described elsewhere.[16,24] A portion of each sample was sealed in a Spectrosil sidearm of the reaction tube so that conductivity measurements could be made without exposing the product to the atmosphere.

Since the samples are both air- and moisture-sensitive and are in powder form, we have developed a contactless

(12) Brus, L. E. *J. Chem. Phys.* **1984**, *80*, 4403.
(13) Henglein, A. *Top Curr. Chem.* **1988**, *143*, 113.
(14) Linsebigler, A.; Lu, G.; Yates, J. T. *Chem. Rev.* **1995**, *95*, 735.
(15) Edwards, P. P.; Woodall, L. J.; Anderson, P. A.; Armstrong, A. R.; Slaski, M. *Chem. Soc. Rev.* **1993**, *22*, 305.
(16) Anderson, P. A.; Armstrong, A. R.; Edwards, P. P. *Angew. Chem.* **1994**, *106*, 669; *Angew. Chem., Int. Ed. Engl.* **1994**, *33*, 641.
(17) Anderson, P. A.; Woodall, L. J.; Porch, A.; Armstrong, A. R.; Hussain, I.; Edwards, P. P. *Mater. Res. Soc. Symp. Proc.* **1995**, *384*, 9.
(18) Edwards, P. P.; Anderson, P. A.; Woodall, L. J.; Porch, A.; Armstrong, A. R. *Mater. Sci. Eng. A*, in press.
(19) Hussain, I.; Gameson, I.; Anderson, P. A.; Edwards, P. P.; Dyer, A. *J. Chem. Soc., Dalton Trans.* **1996**, 775.
(20) Kelly, M. J. *Int. J. Electron.* **1993**, *75*, 27.
(21) Kelly, M. J. *J. Phys.: Condens. Matter* **1995**, *7*, 5507.
(22) Anderson, P. A.; Edwards, P. P. *J. Am. Chem. Soc.* **1992**, *114*, 10608.
(23) Armstrong, A. R.; Anderson, P. A.; Edwards, P. P. *J. Solid State. Chem.* **1994**, *111*, 178.
(24) Armstrong, A. R.; Anderson, P. A.; Edwards, P. P., manuscript in preparation.

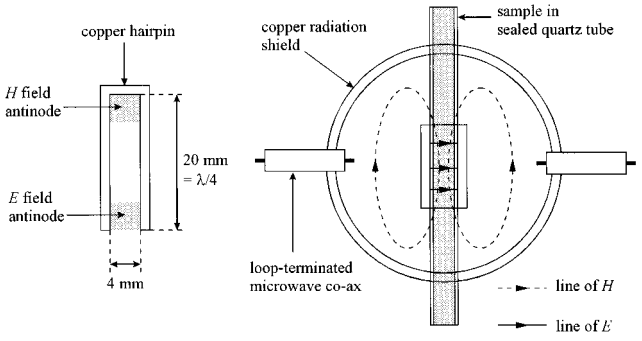

Figure 2. Schematic diagram of the 3 GHz copper hairpin resonator, illustrating the regions of electric and magnetic field antinodes. The resonator is coupled via two coaxial lines terminated in loops, and measurements are performed in transmission using a 8720 HP network analyzer in the temperature range 10−295 K.

microwave cavity perturbation technique based on a quarter-wave copper hairpin resonator at 3 GHz[25] to measure the conductivity. This resonator has well-defined antinodes of microwave electric and magnetic fields into which we can insert the sample. At room temperature the unloaded quality factor of the resonator is around 2000, increasing to over 4000 below 20 K, which is large for its small volume (about 0.8 cm^3). This allows us to make sensitive measurements of the microwave losses owing to the large filling factor of the sample in the resonator. A schematic diagram of the resonator is shown in Figure 2.

The powder grains of the zeolite are small enough (each with a volume of 1−100 μm^3) for us to assume that the mean grain size is much less than the microwave skin depth at these high frequencies. In this limit the measured resonant bandwidth contribution of the zeolite is proportional to the zeolite conductivity when the sample is placed in either the magnetic or electric field antinodes. Previously, we have performed measurements with samples placed in the high microwave magnetic field region of the resonator.[17,18] To estimate absolute values of the conductivity in the case of eddy current dissipation for samples placed in the magnetic field requires a detailed knowledge of the volume size distribution and the shapes of the powder grains. These factors are hard to establish experimentally, so here we will concentrate on the measurements of K_x/K_9-L samples placed in the microwave electric field antinode of the resonator, the results of which are somewhat easier to analyze. The room-temperature resonator responses are shown in Figure 3, where for each sample we plot the microwave power transmitted through the resonator as a function of frequency. The effects of increasing the amount of potassium are an increased bandwidth, due to the increase of the conductivity σ, and a decreased resonant frequency due to the increase of the relative permittivity ϵ'.

Since the zeolite grains are randomly oriented relative to the applied electric field, we adopt a simple model of isotropic spherical dielectric grains with a volume filling factor β to obtain estimates of the complex dielectric constant $\epsilon = \epsilon' - i\epsilon'' \equiv \epsilon' - i\sigma/\omega\epsilon_0$, where σ is the grain conductivity. We assume that local field corrections are small, which is valid for low values of ϵ'. In the limit of small β we find that the resonant frequency shift Δf is approximately

$$\Delta f \approx -3f\frac{\epsilon' - 1\ \beta V_S}{\epsilon' + 2\ V_{res}}$$

where V_S is the sample volume and V_{res} is the resonator volume. The sample conductivity is related to the contribution of the sample to the half-power resonant bandwidth Δf_B by the approximate formula

$$\sigma \approx \frac{\pi}{3}(2 + \epsilon')\epsilon_0 \Delta f_B \frac{V_{res}}{\beta V_S}$$

The results for $\epsilon = \epsilon' - i\epsilon''$ and σ as a function of potassium content at room temperature are listed in Table 1. Since the losses are additive, we can find the conductivity contribution σ' due to the addition of potassium by subtracting the conductivity of the host zeolite from each value of σ. The main errors in the values in Table 1 arise from uncertainties in the volume filling factor β of the sample, which we estimate to be between 30 and 40%. Errors due to variations in the grain shapes are not large and are accommodated within our uncertainty of β.

The values of ϵ' increase slightly with increasing metal content but remain fairly small, resulting in small local field corrections, implicit in our analysis. Interestingly, the conductivity of sample K_9/K_9-L is too high to measure using our technique at room temperature, so we quote a lower limit of 0.5 Ω^{-1} m^{-1}, which represents the point at which the microwave resonance disappears into the background noise (see Figure 3).

Table 1. Values for the Complex Permittivity $\epsilon = \epsilon' - i\epsilon''$ and Conductivity σ for the Series K_x/K_9-L at 295 K[a]

sample	ϵ'	ϵ''	σ (Ω^{-1} m^{-1})
K_9-L	1.7 ± 0.1	0.0015 ± 0.0003	(2.4 ± 0.5) × 10^{-4}
K_1/K_9-L	1.8 ± 0.2	0.0025 ± 0.0005	(4.1 ± 0.8) × 10^{-4}
K_3/K_9-L	2.0 ± 0.2	0.009 ± 0.002	(1.5 ± 0.3) × 10^{-3}
K_5/K_9-L	2.7 ± 0.4	0.25 ± 0.06	0.04 ± 0.01
K_7/K_9-L	3.0 ± 0.5	0.5 ± 0.1	0.07 ± 0.02
K_9/K_9-L		>3	>0.5

[a] No value for ϵ' is quoted for K_9/K_9-L since no resonance is measurable at room temperature for this sample.

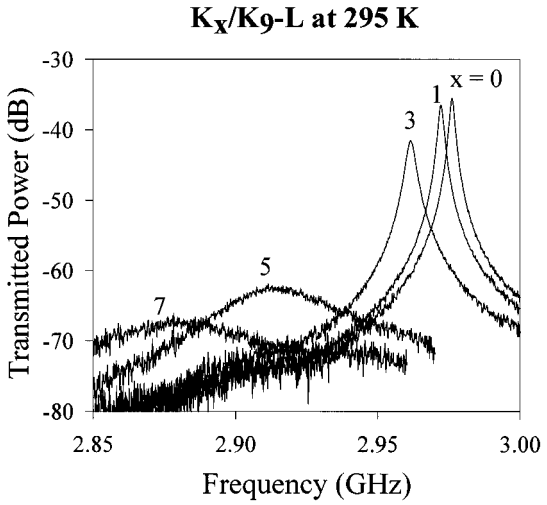

Figure 3. Transmitted microwave power as a function of temperature for various samples of $K_x$$K_9$-L at 295 K. The response of sample K_9/K_9-L is not shown since the sample is too dissipative to observe a resonance at room temperature.

(25) Waldram, J. R.; Porch, A.; Cheah, H.-M. *Physica C* **1994**, *232*, 189.

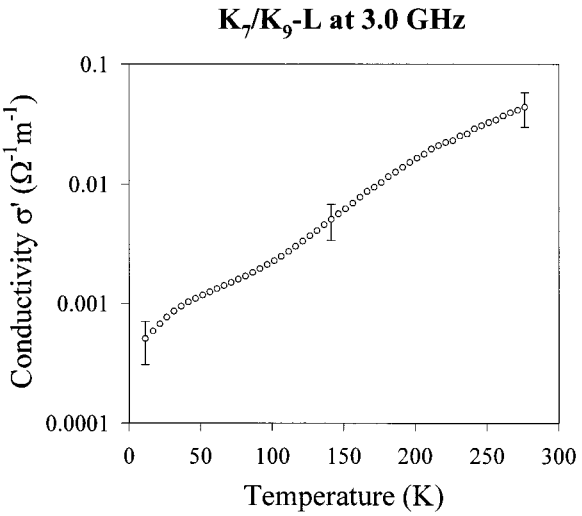

Figure 4. Temperature dependence of the conductivity associated with the addition of potassium $\sigma'(T)$ of sample K_7/K_9-L; note that $\sigma'(T)$ decreases by a factor of around 100 between 280 and 10 K, unlike for a metallic conductor where one would expect that $\sigma'(T) \propto 1/T$.

If these samples were metallic conductors in the conventional sense, then we would expect σ' to increase as $1/T$ for decreasing temperature T (for temperatures above the characteristic Debye temperature of the solid. We plot $\sigma'(T)$ in the range 10−280 K in Figure 4 for sample K_7/K_9-L. We choose this sample since its conductivity is large at room temperature but not too large so as to make the sample bandwidth unmeasurable (as in the case of K_9/K_9-L). We see that $\sigma'(T)$ decreases by a factor of around 100 between 280 and 10 K to reach a value of around 5×10^{-4} Ω^{-1} m^{-1}, similar to the conductivity of the host zeolite at room temperature. We observe similar behavior for $\sigma'(T)$ of sample K_9/K_9-L below 130 K (we cannot measure $\sigma'(T)$ above this temperature for the reasons described above). Despite an increase in room-temperature conductivity of around 5 orders of magnitude caused by the introduction of potassium into zeolite L, the temperature dependence $\sigma'(T)$ does not resemble that of a conventional metallic conductor. However, the values of σ' attained at room temperature for high potassium content are large for ionic conduction, suggesting that we have been successful in modifying the zeolite to exhibit electronic conduction, albeit thermally activated.

Salt Occlusion in Zeolite X

Over the past few decades, much effort has been directed to the use of zeolites as hosts and supports for the preparation of small metallic clusters and particles. Much of this interest has arisen from the important requirement to produce highly dispersed, efficient and selective catalysts for a wide range of chemical processes.[26] In contrast the study of the electronic properties of such materials is still in its infancy. The standard method of introducing a metal species into a zeolite is ion exchange. Here the charge-balancing cations within the zeolite are exchanged for the cations of the desired metal. Metal clusters or particles (and the H^+ form of the zeolite) are then formed by heating in a hydrogen atmosphere. There are, however, a

(26) Uytterhoven, J. B. *Acta Phys. Chem.* **1978**, *24*, 53.

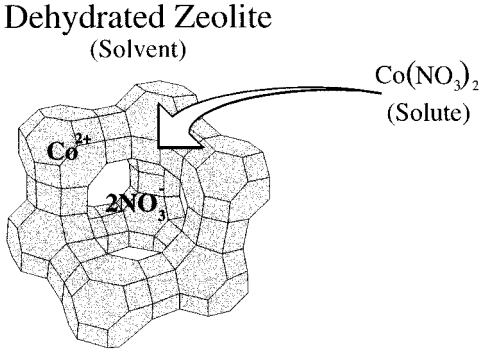

Figure 5. Schematic representation of the occlusion of cobalt nitrate (solute) into zeolite Na-X (solvent).

number of limitations to the ion-exchange method. For example, the total amount of metal introduced into the zeolite is limited by the framework charge. The process is also time consuming and requires strictly controlled conditions (e.g., pH control) to avoid hydrolysis and crystal damage.[27]

One alternative route to ion exchange is the method of salt occlusion initially developed by Barrer and Meier.[28,29] In this process a dehydrated zeolite is heated with a metal salt which becomes incorporated into the zeolite channel system. The sorbed salt species (the solute) is effectively "dissolved" by the zeolite (the solvent) as shown in Figure 5. This occlusion route has two major advantages over the exchange method. First the process takes only a few hours and does not involve the use of large volumes of salt solutions. Second, as both the cationic and anionic species are occluded, in theory the only limit on the amount of materials that can be taken up by the zeolite is the physical size of the void space. Thus the uptake of metal into the zeolite is not limited by the framework charge.

Recently, we have reported the formation of ultrafine magnetic cobalt particles within zeolite Na-X, prepared by the occlusion of $Co(NO_3)_2$ followed by reduction to the metallic state.[19] A tentative reaction scheme for the process is shown below:

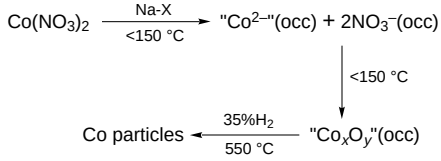

The nature of the occluded Co species before reduction has been investigated, and magnetic susceptibility measurements[19] suggest that Co_3O_4 and not CoO particles are formed within the zeolite. Powder X-ray diffraction of the reduced samples shows a small decrease in the zeolite crystallinity with increasing Co loading. In addition, a broad (111) reflection of fcc cobalt metal is visible in the most highly loaded samples. Analysis of the half-width of the line suggests a Co particle size of ∼15−20 nm. Such particles are clearly too big to be contained within the 1.3 nm zeolite cages. They are not, however, present on the external surface of the zeolite but are thought to occupy locally disrupted

(27) Harjula, R.; Lehto, J.; Pothuis, J. H.; Dyer, A.; Townsend, R. P. *J. Chem. Soc., Faraday Trans.* **1993**, *89*, 971.
(28) Barrer, R. M. *J. Inclusion Phenom.* **1983**, *1*, 105.
(29) Barrer, R. M.; Meier, W. M. *J. Chem. Soc.* **1958**, 299.

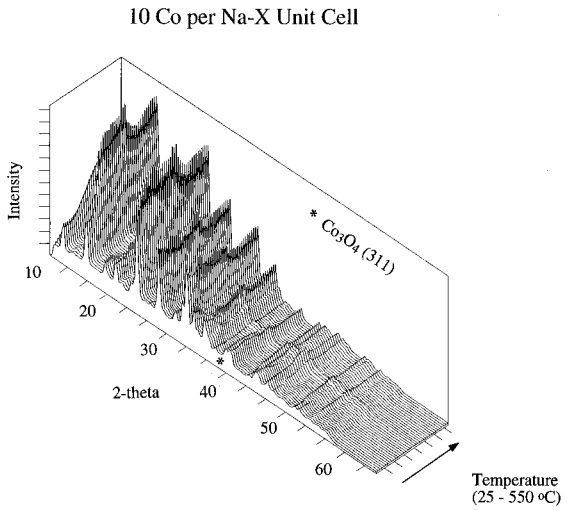

Figure 6. Diffraction patterns of a 10 Co/unit cell occluded sample as a function of temperature. The rapid increase in intensity of the low-angle reflections arises from the dehydration of the zeolite on heating.

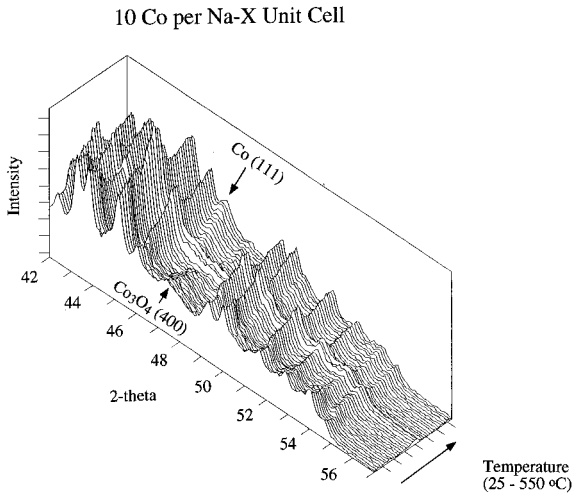

Figure 7. Expanded plot of the X-ray data shown in Figure 6. The presence of small Co_3O_4 particles is indicated by the broad (400) reflection. The formation of nanoscale cobalt metal particles above 300 °C is clearly shown by the growth of a broad (111) reflection.

regions homogeneously dispersed throughout the zeolite matrix. This model is consistent with both XRD and TEM data.[19]

In the present investigation we report some preliminary results from an in situ combined X-ray diffraction/Co EXAFS study on the formation of nanoscale cobalt particles within zeolite Na-X. The aim of this experiment was to determine the form of the occluded oxide species and monitor its subsequent reduction to form nanoscale cobalt particles while observing any changes in the long-range order of the zeolite host. The occluded samples were prepared as reported elsewhere.[19] The experiment was performed at station 9.3 at the Daresbury Laboratory. Pellets 7 mm in diameter, with a typical mass of 40−60 mg, were mounted in a LINKAM furnace into which was passed a 35% H_2/65% N_2 gas stream. X-ray diffraction data were collected on a 120° INEL position-sensitive detector. The usable angular range of this detector was limited to a 2θ range of 10−45 °C by the geometry of the furnace. Co K-edge EXAFS data ($\lambda = 1.608$ Å) were collected in transmission mode. Data were collected on five samples with nominal loadings of 1, 5, 10, 15, and 20 Co/zeolite unit cell. Each sample was heated in a 35% H_2/65% N_2 atmosphere from room temperature to 550 °C at a rate of 1 °C/minute. Five-minute EXAFS and nine-minute X-ray data collections ($\lambda = 1.6423$ Å) were performed alternately as the sample was heated. At the end of the reaction the sample was cooled to room temperature and a final X-ray and EXAFS data collection performed.

Figure 6 shows the X-ray diffraction patterns for the 10 Co sample with increasing temperature. A broad reflection is present at 39.4° (2θ) which persists to 300 °C. This is the (311) reflection of Co_3O_4 which is the most intense peak of this material. As can be seen more clearly in Figure 7, a very broad reflection at 47.3° (2θ) is present in the final diffraction pattern at 550 °C. This is the (111) reflection of cobalt metal. A close examination of the X-ray data shows this feature is visible first at 300 °C, the temperature at which no more Co_3O_4 is detected. A comparison of the room-temperature diffraction patterns collected before and after the reduction reaction shows a reduction in the relative intensities of the diffraction lines at higher 2θ in comparison with those at lower 2θ, which is a clear indication of some loss of long-range order within the zeolite.

Analysis of the EXAFS data on this sample (using the program EXCURV92) confirms that the occluded cobalt species is indeed Co_3O_4. Furthermore, the data can be satisfactorily fitted to a shell model of Co_3O_4 out to 6 Å. Up to a temperature of 225 °C the only change we observe in the fitted parameters is a steady increase in the Debye−Waller thermal parameters. At this point the EXAFS data become more complex. By 275 °C however the data can once again be fitted by a single-phase model but now with CoO. Thus, between 225 and 275 °C the occluded oxide species is reduced to the divalent oxide phase. At 300 °C the data again begin to show the presence of more than one cobalt-containing phase. Satisfactory fits to the data are obtained for a weighted two-phase model containing CoO and Co metal. The relative amount of Co metal in the model increases with increasing temperature from 25% to 350 °C to 75% at 400 °C. Finally by 425 °C only Co metal is detected in the EXAFS data. Fitting the data up to 550 °C shows only a continual increase in the thermal parameters. The unexpected presence of the CoO as detected by EXAFS combined with the absence of any CoO reflections in the X-ray data illustrates the importance of combining two complementary techniques which examine short- and long-range order, respectively. One possible explanation for this anomaly is that the majority of the CoO lines overlap with those of the zeolite and the presence of the broad diffraction lines from small CoO particles are therefore difficult to detect.

Computational Studies

Some years ago Kasai and others[30,31] considered the ability of zeolites to promote a range of chemical processes:

$$Na \rightarrow Na^+ + e^-$$

(30) Kasai, P. H.; Bishop, R. J. *J. Phys. Chem.* **1973**, *77*, 2308.
(31) Rabo, J. A.; Kasai, P. H. *Prog. Solid State Chem.* **1975**, *9*, 1.

$$NaO_2 \rightarrow Na^+ + O_2^-$$

$$N_2O_3 \text{ or } NO + NO_2 \rightarrow NO^+ + NO_2^-$$

$$NaCl \rightarrow Na^+ + Cl^-$$

$$Cu^{2+} \text{ (or } Ni^{2+}) + NO \rightarrow Cu^+ \text{ (or } Ni^+) + NO^+$$

As written, many of these reactions are endothermic, but all have been found to proceed within zeolite crystals. Kasai and co-workers noted that the common feature of these processes was that each led to an increase in the number of charged species and suggested that the driving force for such reactions was a gain in Madelung energy achieved through filling the voids in highly ionic (exchangeable cations coordinating to an anionic framework) zeolite crystals with suitably arranged charged species.

In an effort to move toward a more rigorous explanation for the driving force behind the processes listed above—two of which we have exploited in this work—we have performed detailed calculations of cation solvation energies. We have considered explicitly the dissolution and ionization of alkali metals, but the results are also of relevance to the dissolution of ionic salts in zeolites (salt occlusion).

The dissolution of alkali metals in zeolitic hosts raises a number of fundamental questions. The basic process of dissolution is, as we have seen:

$$M \rightarrow M^+_{solv} + e^-_{trap}$$

where by M^+_{solv} we indicate a "solvated" cation, i.e., a cation stabilized by its interaction with the polar zeolite framework, and where e^-_{trap} represents the corresponding ionized electron trapped at a site elsewhere in the lattice. Assuming the metal is introduced from the gas phase, the energy of this process can be written as

$$E = E_I - E_{solv} - E_{trap}$$

where E_I is the ionization potential of the metal atom and E_{solv} and E_{trap} represent the solvation and trapping energies, respectively. Trapping energies may generally be expected to be relatively low, as shown in recent work by Ursenbach et al.,[32] who calculated (using pseudopotential LDA techniques) a value of ~1 eV for the energy of electron trapping (as an Na_4^{3+} cluster) within a sodalite cage in zeolite Y. Since ionization energies for alkali-metal atoms are in the range 4−5 eV, it is clear that the solvation energy E is dependent on the balance between E_I and E_{solv}.

The calculation of solvation energies is a classical problem in physical chemistry. In the present case it is, however, possible to undertake reliable calculations since the structure of the zeolite lattice is well defined (unlike that of a liquid) and because reliable potentials are available for the interaction between the zeolite framework and exchangeable cations and between ions within the zeolite framework. We have therefore exploited this possibility by performing two sets of calculations: (i) solvation energies of Na^+ or K^+ ions within a model faujasite framework and a purely siliceous analogue, which enable us to assess the effect of aluminum content on the solvation energies; (ii) the energetics of the K^+ ion within zeolite L, allowing us to identify low-energy sites within the framework as well as indicating the structure sensitivity of the solvation energies.

Table 2. Calculated Cation Solvation Energies in the Faujasite Structure Obtained from Mott−Littleton Simulations

cation	atomic ionization potential (eV)	E_{solv} (eV) pure silica faujasite	E_{solv} (eV) sodium zeolite Y
Na^+	5.14	−3.33	−4.21
K^+	4.34	−2.75	−3.35

Our calculations used the standard "Mott−Littleton" techniques[33,34] available in the GULP code,[35] which allowed us to model atomistically the response of the surrounding lattice to the perturbation created by the inserted ion. To this end minimization procedures were used to obtain the minimum energy configuration of a region of lattice (containing typically 300 ions) around the ion; polarization of the more distant regions were calculated using a quasi-continuum model. These methods have been extensively and successfully applied to model defects in polar crystals.[36] The calculations employed standard Born model potentials (supplemented by O−Si−O bond bending terms), with a shell model treatment of polarizability. The parameterizations employed were those of ref 37 and 38, whose validity in modeling structural and energetic properties of zeolites is well established.

In our calculations on the faujasite systems, the cations were introduced close to the SII site; energy minimization was performed with respect to the coordinates of the inserted ion and then the surrounding lattice ions as summarized above. The zeolite was modeled by a faujasite framework in which Al and Si atoms were distributed over T sites to give a resulting Si/Al ratio of 1.4. The charge-compensating extraframework Na^+ ions were distributed over the SII sites, and full lattice energy minimization was undertaken prior to inserting the additional cation. The calculation yields directly the energy change associated with insertion of the cation from infinity into the *relaxed* lattice, i.e., E_{solv} as defined above.

The resulting values for E_{solv} are reported in Table 2, which also gives relevant ionization potentials. The first striking feature of the results is that the solvation energy for the purely siliceous faujasite is substantially lower than that of the corresponding ionization potentials. In particular the *differences* of ~2 eV between the ionization (E_I) and solvation energies (E_{solv}) are too large to be overcome by the trapping energy (E_{trap}) which as noted above has been calculated as ~1 eV. As a consequence we would not expect sodium or potassium vapor to dissolve and ionize in high-silica faujasite. The

(32) Ursenbach, C. P.; Madden, P. A.; Stich, I.; Payne, M. C. *J. Phys. Chem.* **1995**, *99*, 6697.

(33) Mott, N. F.; Littleton, M. J. *Trans. Faraday Soc.* **1938**, *34*, 389.

(34) Catlow, C. R. A.; Mackrodt, W. C. In *Computer Modelling of Solids*; Catlow, C. R. A., Mackrodt, W. C., Eds.; Springer: Berlin, 1982; Lecture Notes in Physics, Vol. 166, p 1.

(35) Gale, J. D. GULP Code, Royal Institution of Great Britain, 1993.

(36) Catlow, C. R. A. *Annu. Rev. Mater. Sci.* **1986**, *16*, 517.

(37) Sanders, M. J.; Leslie, M.; Catlow, C. R. A. *J. Chem. Soc., Chem. Commun.* **1984**, 1271.

(38) Jackson, R. A.; Catlow, C. R. A. *Mol. Sim.* **1988**, *1*, 207.

Table 3. Calculated Cation Solvation Energies in the LTL Structure Obtained from Mott−Littleton Simulations

	$E_{solv}(K^+)$/eV	
cation site[a]	in siliceous LTL	in K_9-L
$^1/_3$, $^2/_3$, $^1/_2$	−2.87	−4.54
0, $^1/_2$, $^1/_2$	−2.57	
$^1/_3$, $^2/_3$, 0	−0.44	−2.33
0, $^1/_2$, 0	−1.67	
0, 0.32, 0	−3.27	−3.09

[a] Crystallographic coordinates are given with respect to the space group *P*6/*mmm*, and are consistent with the structural determinations in refs 39 and 40.

result accords with the general experimental observation that significant quantities of alkali metals cannot be loaded into high-silica zeolites. The solvation energies for these systems are simply too small to outweigh the ionization energies. Very different results were found in the case of zeolite Y. The calculated solvation energies are significantly higher—*sufficiently close to the ionization energies to result in ionization given values for* E_{trap} *of ~1 eV*. It is important to note that framework relaxation is *essential* in achieving the requisite values of the solvation energy. Values for the solvation energy are ~2 eV lower when the cations are inserted in an unrelaxed framework. Without framework relaxation, ionization would not occur. Our finding that ionization is exothermic for Na and K insertion in zeolite Y is consistent with experimental observations on this system and with the general observation that appreciable aluminum content is needed if alkali metals are to dissolve and ionize in zeolites. The reason for the contrast with the purely siliceous systems is simple: the negatively charged aluminosilicate frameworks lead to a higher solvation energy than obtained for the purely siliceous systems.

Two sets of calculations have been carried out on the zeolite L structure. In the first, the solvation energy of a potassium ion was determined at each of five crystallographically distinct sites within the completely siliceous zeolite L structure. The simulations were then repeated for three of the sites but within a framework of composition $K_9Si_{27}Al_9O_{72}$ (K_9-L). Aluminum was distributed randomly over T sites according to Löwenstein's rule, and potassium ions were distributed randomly over the experimentally observed extraframework sites.[39,40] The results are given in Table 3. Two points in general stand out: (i) there is a strong site dependence of the energies (the results for K_9-L will moreover be dependent on the Al and cation distribution—a factor that is beyond the current scope of our investigation); (ii) the energies are generally more favorable, by about ~2 eV, in K_9-L than in the siliceous isomorph. In fact the solvation energy in the former for the first site would be sufficient to lead to the ionization of potassium without any contribution from the electron trapping energy E_{trap}. The possibility of such high solvation energies is significant with regard to the experimental goal of preparing compounds containing very weakly bound, or indeed delocalized, electron states.

(39) Newsam, J. M. *J. Phys. Chem.* **1989**, *93*, 7689.
(40) Barrer, R. M.; Villiger, H. *Z. Kristallogr.* **1969**, *142*, 82.

Concluding Remarks

In this work we have illustrated two examples of the use of zeolitic hosts for the synthesis of matrix-bound electronic structures. In the first example, the sorption of potassium metal in zeolite L leads to the controlled doping of both excess cations and electrons into the host matrix. In the first quantitative application of a contactless microwave cavity conductivity measurement to compounds of this type, we have observed an increase in room temperature conductivity of around 5 orders of magnitude on potassium doping. The magnitude of the room-temperature conductivity and the strong temperature dependence suggest that we have been successful in modifying the zeolite to exhibit significant thermally activated electronic conduction. We believe that such materials are close to a matrix-bound insulator−metal transition.

In the second example, the dissolution or occlusion of a metal salt, in this case cobalt nitrate, in zeolite X, facilitates the preparation of nanoscale ferromagnetic particles of cobalt metal. A combined X-ray/EXAFS study has provided valuable insights into this process. EXAFS has confirmed that the occluded Co species is Co_3O_4 and that this is stable to 225 °C. Beyond this temperature it is rapidly reduced by hydrogen gas to CoO. From 300 °C, Co metal particles are formed and this reduction step is complete by 425 °C. X-ray diffraction confirms that Co particles begin to form at 300 °C and that this process coincides with some reduction in the overall crystallinity of the zeolite.

Finally, in an effort to move toward a deeper understanding of the two related chemical processes exploited in the above examples, we have performed detailed calculations of cation solvation energies. Our results demonstrate that calculations of this type will prove an invaluable tool in predicting future candidate systems for study, in particular those that may contain weakly bound or metallic electron states.

Acknowledgment. We thank the EPSRC, The Royal Society, and Alcan Chemicals Ltd. for their support of this work.

CM960167K